Title

Effective one-particle energies from generalized Kohn–Sham random phase approximation: A direct approach for computing and analyzing core ionization energies

Journal

The Journal of Chemical Physics, 151(13)

ISSN

0021-9606

Authors

Voora, Vamsee K
Galhenage, Randima
Hemminger, John C
et al.

Publication Date

2019-10-07

DOI

10.1063/1.5116908

Peer reviewed

Effective one-particle energies from generalized Kohn–Sham random phase approximation: A direct approach for computing and analyzing core ionization energies

Vamsee K. Voora,[1, 2, a)] Randima Galhenage,[1] John C. Hemminger,[1] and Filipp Furche[1, b)]

[1)] *Department of Chemistry, University of California, Irvine, 1102 Natural Sciences II, Irvine, California 92697-2025, USA*

[2)] *Department of Chemical Sciences, Tata Institute of Fundamental Research, Homi Bhabha Road, Colaba, Mumbai 400005, India*

(Dated: 1 September 2019)

Generalized-Kohn-Sham (GKS) orbital energies obtained self-consistently from the random phase approximation energy functional with semicanonical projection (spRPA) were recently shown to rival the accuracy of *GW* quasiparticle energies for valence ionization potentials. Here we extend the scope of GKS-spRPA correlated one-particle energies from frontier-orbital ionization to core orbital ionization energies, which are notoriously difficult for *GW* and other response methods due to strong orbital relaxation effects. For a benchmark consisting of 23 1s core electron binding energies (CEBEs) of second-row elements, chemical shifts estimated from GKS-spRPA one-particle energies yield mean absolute deviations from experiment of 0.2 eV, which is significantly more accurate than standard *GW* and comparable to Δ self-consistent field theory without semi-empirical adjustment of the energy functional. For small ammonia clusters and cytosine tautomers, GKS-spRPA based chemical shifts capture subtle variations in covalent and non-covalent bonding environments; GKS-spRPA 1s CEBEs for these systems agree with equation-of-motion coupled cluster singles and doubles and ADC(4) results within 0.2-0.3 eV. Two perturbative approximations to GKS-spRPA orbital energies, which reduce the scaling from $\mathcal{O}(N^6)$ to $\mathcal{O}(N^5)$ and $\mathcal{O}(N^4)$, are introduced and tested. We illustrate the application of GKS-spRPA orbital energies to larger systems by using oxygen 1s CEBEs to probe solvation and packing effects in condensed phases of water. GKS-spRPA predicts a lowering of the oxygen 1s CEBE of approximately 1.6-1.7 eV in solid and liquid phases, consistent with liquid-jet XPS and gas phase cluster experiments. The results are rationalized by partitioning GKS-spRPA electron binding energies into static, relaxation, and correlation parts.

[a)]Electronic mail: vamsee.voora@tifr.res.in

[b)]Electronic mail: filipp.furche@uci.edu

I. INTRODUCTION

The change in core electron binding energies (CEBEs) due to changes in the local chemical environment, also known as the chemical shift, provides valuable information about the electronic structure and chemical bonding of atoms and molecules in gas, liquid, and solid phases.[1] Experimentally, molecular CEBEs are accessible by X-ray photoelectron spectroscopy (XPS); recent advances in high vapor pressure liquid-jet experiments have extended the scope of XPS measurements to solvents such as water and ammonia.[2–4] Chemical shifts of solvated molecules in liquid water provide important clues for concentration profiles near the vapor-liquid interface.[5–8]

Ab initio calculation of core ionization potentials provides a means to predict CEBEs and rationalize chemical shifts.[9] Theoretical modeling can help analyze the experimentally measured peaks, which are often broadened due to vibrational effects and sometimes unresolved due to background scattering processes; the vertical ionization energy is then interpreted using various fitting schemes.[10] Compared to modeling valence electron ionization potentials, core ionization poses special challenges due to large relaxation effects, high ionization energies, and strong relativistic effects for heavy nuclei.[11–14] The widely used delta (Δ) methods obtain CEBEs from separate iterative and/or self-consistent total energy calculations of the (N)-electron ground state and an $(N-1)$-electron core excited state; for example, ΔSCF, refers to the use of Hartree–Fock (HF) self-consistent field (SCF) theory for individual energy calculations.[15,16] In addition to one-electron electrostatic and exchange effects, Δ methods include relaxation effects, which are a significant fraction of the CEBE and the most important contribution to the chemical shifts.[15,16] Correlation effects can be included by using various density functional approximations (DFAs) or post-HF methods to compute the two states.[17–19] ΔSCF and ΔDFAs have a low computational cost of $\mathcal{O}(N^3)$, but suffer from variational collapse and convergence issues[20] in the absence of additional constraints.

Direct or response methods compute the CEBEs using the energy functional of N-electron system only, and hence avoid similar convergence-related issues as Δ methods. Direct approaches such as the algebraic diagrammatic construction (ADC)[21] and equation-of-motion coupled cluster (EOM-CC),[22,23] include high-order correlation effects.[24–26] However, the steep $\mathcal{O}(N^7)$ computational cost of ADC(4) hampers large-scale applications, even with additional approximations such as core-valence separation (CVS)[24,27]. Quasiparticle methods

based on Hedin's equations[28,29] use the one-body Green's function as basic variable. With an $\mathcal{O}(N^5)$ scaling, G_0W_0 is the simplest among the quasiparticle methods but requires nonlinear eigenvalue iterations. The linearized-G_0W_0 approach (*lin*-G_0W_0)), avoids the iterations, but produces errors in CEBEs of the order of several eVs.[30,31] When based on a noninteracting Kohn-Sham (KS)[32] reference determinant, G_0W_0 and *lin*-G_0W_0 may be viewed as post-KS approaches. As such, they depend on the KS potential and the density matrix, which can render the results sensitive to the choice of a specific approximate functional. While semi-empirical adjustment of the hybrid exchange mixing parameter was found to substantially improve CEBEs from *lin*-G_0W_0,[31] the optimum amount of hybrid exchange varies from 35–40% for valence ionization[33,34] to 50% or more for core ionization.[31] This initial state dependence is remedied to some extent by self-consistent GW methods such as quasiparticle GW[35] and self-consistent GW,[28] but apart from the overhead for carrying out multiple iterations, these nonlinear iterative methods are limited by pervasive initial-state dependence and spurious solutions.[36–38]

On the other hand, effective one-particle theories such as the HF method, and KS and generalized KS (GKS)[39] approaches to density functional theory (DFT) provide one-particle energies as eigenvalues of a self-adjoint, energy-independent single-particle Hamiltonian. KS approaches use a local or semi-local potential in the single-particle Hamiltonian while GKS approaches use a non-local one. These one-particle-energies or orbital-energies, which can be related to derivatives of an energy functional w.r.t occupation numbers of the one-particle states,[40,41] can provide meaningful estimates of ionization energies directly. The meaning of orbital-energies in HF theory is well established through the Koopmans theorem (KT) which states that all orbital energies are related to approximate IPs; correlation and relaxation effects are neglected in this approach.[42] While lowest ionization energies are well estimated using HF orbital energies, due to cancellation of correlation and relaxation effects, core-orbital energies overestimate the actual CEBEs by tens of eVs due to large relaxation effects compared to correlation effects. Within the KS and GKS schemes the highest occupied molecular orbital (HOMO) energy is related to negative of the ionization potential.[43,44] In addition, within the GKS scheme, the lowest unoccupied molecular orbital energy is related to negative of electron affinity.[41,45] For both schemes, the relevance of other orbital energies w.r.t ionization potentials is unclear. Core orbital energies from semi-local functionals, such as PBE[46] in the KS framework, and hybrid functionals, such as B3LYP[47,48] in the GKS

framework, underestimate the CEBEs by tens of eVs.[30,49] The orbital energy estimation from HF, PBE and B3LYP energy functionals requires only $\mathcal{O}(N^3)$steps.

Recently, a GKS scheme was applied to semicanonical projected random phase approximation (spRPA) energy functional, which includes non-local exact-exchange and correlation.[50] The orbital energies from GKS-spRPA were found to approximate the frontier ionization potentials and fundamental gaps of atoms and molecules more accurately than semi-local DFAs or G_0W_0 and correct the spurious behavior of semi-local DFAs for negative ions. Here we assess the accuracy of GKS-spRPA orbital energies for CEBEs. A partitioning scheme for analyzing the chemical shifts is proposed to core-orbital energies in GKS-spRPA, and helps rationalize its applicability for CEBEs.

In Sec. II, we summarize the GKS-spRPA method and present a diagonal-approximation to GKS-spRPA to reduce the computational cost as well as a partitioning scheme for analyzing different contributions to GKS-spRPA orbital energies. Computational details are given in Sec. III, followed by benchmarks for CEBEs and chemical shifts based on experimental results and correlated wavefunction methods in Sec. IV A. In Sec. IV B, we demonstrate how GKS-spRPA CEBEs can be used in conjunction with XPS measurements to probe the local chemical environment of water. Conclusions are presented in Sec. V.

II. THEORETICAL BACKGROUND

A. Generalized Kohn–Sham semicanonical projected random phase approximation

In the GKS-spRPA method, the spRPA energy functional

$$E^{\mathrm{spRPA}}[\mathrm{D}, \tilde{\mathrm{H}}_0^{\mathrm{KS}}[\mathrm{D}]] = E^{\mathrm{HF}}[\mathrm{D}] + E^{\mathrm{C\ spRPA}}[\mathrm{D}, \tilde{\mathrm{H}}_0^{\mathrm{KS}}[\mathrm{D}]] \tag{1}$$

is minimized with respect to the non-interacting GKS density matrix

$$\mathrm{D} = \sum_{\lambda} \mathrm{P}_\lambda \mathrm{n}_{\lambda\lambda'} \mathrm{P}_\lambda. \tag{2}$$

D is constrained to be normalized to N electrons and have eigenvalues between 0 and 1. P_λ denotes orthogonal projectors belonging to blocks of KS orbitals with degenerate occupation numbers, and $\mathrm{n}_{\lambda\lambda'} = \mathrm{n}_\lambda \delta_{\lambda\lambda'}$ is diagonal, with n_λ denoting occupation number matrices.[50]

For integer KS occupations n_λ has eigenvalues $n_\lambda = 1, 0$. The semicanonical projected (sp) KS Hamiltonian

$$\tilde{\mathrm{H}}_0^{\mathrm{KS}} = \sum_\lambda \mathrm{P}_\lambda \mathrm{H}_0^{\mathrm{KS}} \mathrm{P}_\lambda, \tag{3}$$

contains only the diagonal ($\lambda = \lambda'$) blocks of the KS Hamiltonian

$$\mathrm{H}_{0,ij}^{\mathrm{KS}} = \mathrm{h}_{ij} + \sum_{pq} \mathrm{V}_{ipjq} \mathrm{D}_{pq} + \mathrm{V}_{ij}^{\mathrm{XC}}[\mathrm{D}] \; . \tag{4}$$

h is the one-electron Hamiltonian, the second term denotes the Hartree or Coulomb potential and V^{XC} is the exchange-correlation potential. The subscripts $i, j, ..$ denote orbital indices. V is the matrix of two-electron integrals

$$\mathrm{V}_{pqrs} = \int\int d^3r_1 d^3r_2 \frac{\phi_p^*(\mathbf{r}_1)\phi_q^*(\mathbf{r}_2)\phi_r(\mathbf{r}_1)\phi_s(\mathbf{r}_2)}{|\mathbf{r}_1 - \mathbf{r}_2|} \; . \tag{5}$$

The first term in Eq. 1 is the HF energy evaluated at a given density matrix and the second term is the RPA correlation energy[51–55]

$$E^{\mathrm{C\ spRPA}} = \frac{1}{2}\Im \int_{-\infty}^{\infty} \frac{d\omega}{2\pi} \langle \ln(1 - \Pi_0(\omega)\mathrm{V}) + \Pi_0(\omega)\mathrm{V} \rangle. \tag{6}$$

$\Pi_0(\omega)$ denotes the (time-ordered) non-interacting Kohn-Sham (KS) propagator; brackets stand for traces. $\Pi_0(\omega)$ factorizes,[56]

$$\Pi_{0\,pqrs}(\omega) = \int_{-\infty}^{\infty} \frac{d\omega'}{2\pi i} \mathrm{G}_{0\,ps}(\omega') \mathrm{G}_{0\,qr}(\omega' - \omega), \tag{7}$$

into a product of one-particle semicanonical KS Green's functions

$$\mathrm{G}_0(\omega) = \mathrm{n}^{1/2}(\omega - \tilde{\mathrm{H}}_0 - i\eta)^{-1}\mathrm{n}^{1/2} + (1 - \mathrm{n})^{1/2}(\omega - \tilde{\mathrm{H}}_0 + i\eta)^{-1}(1 - \mathrm{n})^{1/2}; \tag{8}$$

where the subscripts $p, q, ...$ represent general orbital indices, and η is small positive contour distortion.

Requiring stationarity of the spRPA energy functional under variations of D leads to the canonical GKS SCF equations

$$\mathrm{H}^{\mathrm{spRPA}}[\mathrm{D}]\phi_p = \varepsilon_p^{\text{GKS-spRPA}} \phi_p, \tag{9}$$

which are solved iteratively. ϕ_p and $\epsilon_p^{\text{GKS-spRPA}}$ are the one-particle GKS-spRPA orbitals and orbital energies, and $\mathrm{H}^{\mathrm{spRPA}}[\mathrm{D}]$ is the density matrix derivative of the RPA energy functional

$$\mathrm{H}^{\mathrm{spRPA}}[\mathrm{D}] = \frac{\delta E^{\mathrm{spRPA}}[\mathrm{D}]}{\delta \mathrm{D}} = \mathrm{H}^{\mathrm{HF}}[\mathrm{D}] + \mathrm{V}^{\mathrm{C\ spRPA}}[\mathrm{D}] \tag{10}$$

where, the first term is the Fock matrix, and the second term is the RPA correlation potential

$$\mathrm{V}^{\mathrm{C\ spRPA}}[\mathrm{D}] = \int_{-\infty}^{\infty} \frac{d\omega}{2\pi} \Sigma^{\mathrm{C}}(\omega) \frac{\delta \mathrm{G}_0}{\delta \mathrm{D}} \, . \tag{11}$$

The functional derivative of G_0 is a rank-four tensor, and its properties are described in Appendix B of Ref. 50. The frequency-dependent RPA correlation self-energy is given as

$$\Sigma^{\mathrm{C}}(\omega) = -\int_{-\infty}^{\infty} \frac{d\omega}{\pi i} \mathrm{W}^{\mathrm{C}}(\omega') \mathrm{G}_0(\omega' - \omega) \, . \tag{12}$$

$\mathrm{W}^{\mathrm{C}}(\omega) = -\delta E^{\mathrm{C\ RPA}}/\delta \Pi_0(\omega)$, is the frequency ($\omega$)-dependent screened-Coulomb interaction matrix

$$\mathrm{W}^{\mathrm{C}}(\omega) = \mathrm{V}[1 - \Pi_0(\omega)\mathrm{V}]^{-1} \Pi_0(\omega) \mathrm{V} \, . \tag{13}$$

The inverse matrix in Eq. 13 is the frequency-dependent dielectric screening matrix[57]

$$\kappa(\omega) = 1 - \Pi_0(\omega)\mathrm{V}. \tag{14}$$

B. Diagonal approximation to GKS-spRPA

$\mathrm{H}^{\mathrm{spRPA}}[\mathrm{D}]$ has the following block-matrix structure

$$\mathrm{H}^{\mathrm{spRPA}}[\mathrm{D}] = \begin{pmatrix} \mathrm{H}^{\mathrm{spRPA}}_{\underline{11}} & \mathrm{H}^{\mathrm{spRPA}}_{\underline{10}} \\ \mathrm{H}^{\mathrm{spRPA}}_{\underline{01}} & \mathrm{H}^{\mathrm{spRPA}}_{\underline{00}} \end{pmatrix} \, . \tag{15}$$

The underlined subscripts of the blocks correspond to occupation-number degeneracy. The occupied-virtual blocks, $\mathrm{H}^{\mathrm{spRPA}}_{\underline{10}}$ and $\mathrm{H}^{\mathrm{spRPA}}_{\underline{01}}$, correspond to the orbital-rotation gradient, whereas the $\mathrm{H}^{\mathrm{spRPA}}_{\underline{11}}$ and $\mathrm{H}^{\mathrm{spRPA}}_{\underline{00}}$ blocks are relevant to the ionization potentials and electron affinities, respectively.

At the stationarizing solution, the occupied-virtual block vanishes, thus decoupling the occupied-occupied and virtual-virtual (vv) blocks. The computational cost for evaluating the complete oo block is $\mathcal{O}((N^{occ})^3 N^{virt} (N^{aux})^2)$ within the resolution-of-the-identity (RI) approximation, and imaginary frequency integration.[54] N^{aux}, N^{occ} and N^{virt} denote the total number of auxiliary functions, occupied and virtual orbitals, respectively. For frequency integration, we use Clenshaw-Curtis quadrature,[58] and the number of quadrature points is denoted by n_g. The diagonalization of the oo block provides orbital energies that correspond to all principal ionization energies. Since we are interested in the the core-ionization energies

only, which are well-separated from other valence ionization energies, we can assume a diagonal approximation to the occupied-occupied (and virtual-virtual) blocks

$$(\mathrm{H}^{\text{d-spRPA}}_{\underline{\lambda\lambda}})_{ij} = \delta_{ij}(\mathrm{H}^{\text{spRPA}}_{\underline{\lambda\lambda}})_{ij} \; . \tag{16}$$

The resulting approximation, called d-GKS-spRPA, has a computational cost of $\mathcal{O}((N^{occ})^2 N^{virt}(N^{aux})^2)$ for computing a single orbital energy of interest, which is an order of magnitude cheaper than computing the full ionization spectrum in GKS-spRPA.

C. Interpretation of one-particle energies from GKS-spRPA

From equations (1),(9) and (15), the GKS-spRPA (or d-GKS-spRPA) orbitals energies has three main components

$$\begin{aligned} \varepsilon_i^{\text{GKS-spRPA}} &= \mathrm{H}^{\text{spRPA}}_{ii}[\mathrm{D}] \\ &= \mathrm{H}^{\text{HF}}_{ii}[\mathrm{D}] + \mathrm{V}^{\mathrm{C,r}}_{ii}[\mathrm{D}] + \mathrm{V}^{\mathrm{C,s}}_{ii}[\mathrm{D}] \; . \end{aligned} \tag{17}$$

where,

$$\begin{aligned} \mathrm{H}^{\text{HF}}[\mathrm{D}] &= \frac{\delta E^{\text{HF}}[\mathrm{D}]}{\delta \mathrm{D}} \\ \mathrm{V}^{\mathrm{C,r}}[\mathrm{D}] &= \frac{\delta E^{\text{c spRPA}}[\mathrm{D}, \tilde{\mathrm{H}}_0^{\mathrm{KS}}[\mathrm{D}]]}{\delta \mathrm{D}} \\ \mathrm{V}^{\mathrm{C,s}}[\mathrm{D}] &= \frac{\delta E^{\text{c spRPA}}[\mathrm{D}, \tilde{\mathrm{H}}_0^{\mathrm{KS}}[\mathrm{D}]]}{\delta \tilde{\mathrm{H}}_0^{\mathrm{KS}}[\mathrm{D}]} \frac{\delta \tilde{\mathrm{H}}_0^{\mathrm{KS}}[\mathrm{D}]}{\delta \mathrm{D}} \; , \end{aligned} \tag{18}$$

$\mathrm{H}^{\text{HF}}[\mathrm{D}]$ is the HF one-particle Hamiltonian, $\mathrm{V}^{\mathrm{C,r}}$ and $\mathrm{V}^{\mathrm{C,s}}$ are the response and static portions of the RPA correlation-potential.

The HF Hamiltonian

$$\mathrm{H}^{\text{HF}}_{ii} = \mathrm{h}_{ii} + \sum_{j=1}^{N_{occ}} (\mathrm{V}_{ijij} - \mathrm{V}_{ijji}) \tag{19}$$

accounts for the static (or frozen) Coulomb and exchange effects that the electron in orbital i "feels" due to all other other electrons. It is the dominant contribution to the CEBEs but not necessarily to chemical shifts as discussed below.

$\mathrm{V}^{\mathrm{C},r}[\mathrm{D}]$ results from the functional derivative of $E^{\text{C RPA}}$ with respect to D at fixed $\tilde{\mathrm{H}}_0^{\mathrm{KS}}$

$$\mathrm{V}^{\mathrm{C,r}}_{ii} = \int_{-\infty}^{\infty} \frac{d\omega}{\pi} \sum_p \mathrm{W}^{C}_{ippi}(\omega) \mathrm{G}_{0\,pp}(\omega + \tilde{\epsilon}_i) \; . \tag{20}$$

$\tilde{\epsilon}_i$ are the eigenvalues of $\tilde{\mathrm{H}}_0^{\mathrm{KS}}$. This term accounts for response of the system due to ionization of an electron. The response effects can be further separated into orbital-correlation (V^{oc}) and orbital-relaxation (V^{or}) components

$$\mathrm{V}^{\mathrm{C,r}}_{ii} = \mathrm{V}^{\mathrm{oc}}_{ii} + \mathrm{V}^{\mathrm{or}}_{ii} \ , \tag{21}$$

where,

$$\begin{aligned}
\mathrm{V}^{\mathrm{oc}}_{ii} &= \int_{-\infty}^{\infty} \frac{d\omega}{\pi} \sum_{p\neq i} \mathrm{W}^{C}_{ippi}(\omega)\mathrm{G}_{0\,pp}(\omega+\tilde{\epsilon}_i) \\
\mathrm{V}^{\mathrm{or}}_{ii} &= \int_{-\infty}^{\infty} \frac{d\omega}{\pi} \mathrm{W}^{C}_{iiii}(\omega)\mathrm{G}_{0\,ii}(\omega+\tilde{\epsilon}_i) \ .
\end{aligned} \tag{22}$$

Our rationale for this partitioning is that upon neglecting screening effects, i.e imposing $\kappa(\omega) = 1$, we obtain the familiar second-order correlation and relaxation contributions from Green's function theory[59–61]

$$\begin{aligned}
\mathrm{V}^{\mathrm{oc(2)}}_{ii} &= \int_{-\infty}^{\infty} \frac{d\omega}{\pi} \sum_{p\neq i} \mathrm{W}^{\mathrm{C(2)}}_{ippi}(\omega)\mathrm{G}_{0\,pp}(\omega+\tilde{\epsilon}_i) \\
\mathrm{V}^{\mathrm{or(2)}}_{ii} &= \int_{-\infty}^{\infty} \frac{d\omega}{\pi} \mathrm{W}^{\mathrm{C(2)}}_{iiii}(\omega)\mathrm{G}_{0\,ii}(\omega+\tilde{\epsilon}_i) \\
\mathrm{W}^{\mathrm{C(2)}} &= \mathrm{V}\Pi_0(\omega)\mathrm{V} \ .
\end{aligned} \tag{23}$$

Thus V^{oc} and V^{or} are screened versions of their second-order counterparts. V^{or} recovers most of the relaxation obtained from Δ approaches, and its computational cost is only $\mathcal{O}(N^{occ}N^{virt}(N^{aux})^2)$ i.e. an order of magnitude less than that of the complete correlation-potential within d-GKS-spRPA.

$\mathrm{V}^{\mathrm{C,s}}$ represents additional static corrections to the potential due to correlation effects, that is "felt" by an electron in the ith orbital

$$\mathrm{V}^{\mathrm{C,s}}_{ii}[\mathrm{D}] = \sum_{j=1}^{N_{occ}} \mathrm{T}_{ij}\mathrm{F}^{\mathrm{HXC}}_{ji} \ . \tag{24}$$

$\mathrm{F}^{\mathrm{HXC}} = \delta\tilde{\mathrm{H}}_0^{\mathrm{KS}}/\delta\mathrm{D}$ is the semi-local Hartree-exchange-correlation kernel. $\mathrm{T} = \delta E^{\mathrm{c\ spRPA}}/\delta\tilde{\mathrm{H}}_0^{\mathrm{KS}}$ is the spRPA correlation density matrix,[50,62] whose matrix elements in the semicanonical basis are given by

$$\mathrm{T}_{ij} = \int_{-\infty}^{\infty} \frac{d\omega}{2\pi} \frac{1}{\omega - \tilde{\varepsilon}_i - i\eta} \Sigma^{\mathrm{C}}_{ij}(\omega) \frac{1}{\omega - \tilde{\varepsilon}_j - i\eta} \ . \tag{25}$$

This term is similar to the static part of the self-energy in Green's function methods such as ADC(4).[63–65] ΔSCF, which is missing correlation effects, and *GW* approximation do not account for this term.[50] The resulting partitioning of the orbital energies,

$$\varepsilon_i^{\text{GKS-spRPA}} = \mathrm{H}_{ii}^{\mathrm{HF}}[\mathrm{D}] + \mathrm{V}_{ii}^{\mathrm{or}}[\mathrm{D}] + \mathrm{V}_{ii}^{\mathrm{oc}}[\mathrm{D}] + \mathrm{V}_{ii}^{\mathrm{C,s}}[\mathrm{D}] \ , \tag{26}$$

will be used to analyze and understand the variations in CEBEs for various cases below. For the case of water-clusters, we use the orbital-relaxation-only approximation, that neglects V^{oc} and $\mathrm{V}^{\mathrm{C,s}}$ terms, and has a computational scaling of $\mathcal{O}(N^{occ}N^{virt}(N^{aux})^2)$.

Unlike post-KS approaches, the GKS-spRPA method is a variational energy minimization technique that removes dependence on the initial state. It however is not functional self-consistent,[50] and hence has a dependency on the choice of the KS potential via $\tilde{\mathrm{H}}_0^{\mathrm{KS}}$. Our approach therefore involves two approximations: (i) the choice of KS potential, $\tilde{\mathrm{H}}_0^{\mathrm{KS}}$, and (ii) the choice of the energy functional for which we choose spRPA. Additional dependence on basis-sets, n_g and η parameters is investigated below.

III. COMPUTATIONAL DETAILS

The GKS-spRPA and d-GKS-spRPA methods were implemented in a local version of TURBOMOLE[66] and are scheduled for a future release. The PBE,[46] BHLYP,[67] TPSS,[68] and *lin*-G_0W_0 calculations were carried out using TURBOMOLE V7.3.[69,70] All calculations were carried out using m5 grids[71] for numerical integration of the KS exchange-correlation potential. Relativistic corrections, tend to be a constant correction for a given element and hence contribute to absolute CEBEs but do not affect the chemical shifts.[72] Except when explicitly stated, all reported CEBEs are non-relativistic. For ammonia clusters, the geometries were obtained from Ref. 73. For the small molecule testset and cytosine tautomers, the geometries were optimized using PBE functional and def2-TZVPP basis-sets. For geometry optimization calculations, an energy convergence criterion of 10^{-7} a.u. and a gradient convergence of 10^{-3} a.u. were used. For GKS-spRPA energy calculations, all electrons were correlated and an energy convergence criterion of 10^{-7} a.u. was used.

To determine the sensitivity of chemical shifts on the choice of basis-sets, DFAs for KS potential, η and n_g, we analyzed the core orbital energies from *d*-GKS-spRPA for a set of molecules shown in Table I. Use of def2-TZVPP, def2-TZVPPD, def2-QZVPP,[74] and a

modified def2-TZVPP basis-sets where the two tight 1s functions are uncontracted, led to MAEs of 0.2 eV, 0.2 eV, 0.3 eV and 0.2 eV, respectively (see SI for further details). Similarly, use of aug-cc-pVTZ and aug-cc-pVQZ[75,76] basis-sets leads to identical MAEs of 0.2 eV. Thus, the choice of basis-sets leads to variations of 0.1 eV in MAE, which is less than the method error. For our studies, which are mainly focused on chemical shifts, we therefore choose to use def2-TZVPP basis-sets, except for large water cluster where a combination of basis-sets is used. Finally, we analyzed the dependence of CEBEs and chemical shifts on the choice of η and n_g. In general, all $\epsilon_i^{\text{GKS-spRPA}}$ values need to be carefully converged w.r.t η and n_g. For a given η value, we found that for cases with nearly degenerate core-orbital energies required a larger number of grid points than non-degenerate cases. For example, with $\eta = 0.01$ a.u., to converge $\epsilon_i^{\text{GKS-spRPA}}$ to within 0.01 eV, N_2 and CO_2 required about 400 grid points whereas the non-degenerate cases, i.e. all other molecules in Table I, required only 60, see SI.

IV. RESULTS AND DISCUSSION

A. Benchmark calculations

1. Small molecules

To test the accuracy of GKS-spRPA and *d*-GKS-spRPA methods, CEBEs and chemical shifts were computed for a small set of molecules for which accurate experimental data were available, see Table I. All calculations were carried out using the def2-TZVPP basis sets. We found that the diagonal approximation to GKS-spRPA changes the CEBEs by <0.01 eV, hence the remaining assessment will be based on the computationally cheaper *d*-GKS-spRPA method. To analyze the impact of choice of potential, we report the results *d*-GKS-spRPA method using PBE and TPSS potentials. For comparison, *lin*-G_0W_0 results based on three different functionals — PBE, TPSS, and BHLYP — are also reported. For CEBEs, *d*-GKS-spRPA based on the PBE potential has a mean absolute error (MAE) of 0.2 eV, which is an order of magnitude less than that of the *lin*-G_0W_0 method using PBE (MAE = 7.9 eV). Using TPSS potential, the MAEs in CEBEs do not change for *d*-GKS-spRPA but the errors for *lin*-G_0W_0 reduce by 1.2 eV. The strong dependence of *lin*-G_0W_0 on the reference orbitals is further exemplified by the BHLYP results showing a dramatic reduction of the MAE to 0.4 eV; BHLYP contains 50% hybrid exchange, which seems to be optimal for CEBEs

TABLE I. Core (1s) electron binding energies (eV) using *lin*-G_0W_0, and core orbital energies from *d*-GKS-spRPA, and GKS-spRPA methods. The mean absolute errors (MAEs) and mean signed errors (MSEs) for non-relativistic CEBEs, CEBEs with relativsitic corrections and chemical shifts w.r.t experimental reference values (Ref.) are also shown. The MSEs are computed as the difference between theoretical and experimental values. For chemical shifts, N(1s) of NH_3, O(1s) of OCS, B(1s) of BCl_3 and C(1s) of HCN are taken as reference. All calculations were carried out using def2-TZVPP basis sets. For d-GKS-spRPA calculations we used $\eta = 0.01$ a.u and $n_g = 400$; PBE and TPSS potential based results are reported. For *lin*-G_0W_0 calculations, we report the results for PBE, TPSS and BHLYP starting points.

Molecule[a]	*lin*-G_0W_0			*d*-GKS-spRPA		Ref.
	PBE	TPSS	BHLYP	PBE	TPSS	
BCl_3	−194.10	−195.18	−200.32	−199.57	−199.72	−199.8[77]
BF_3	−197.80	−198.65	−202.88	−202.28	−202.43	−202.8[77]
H**C**N	−287.02	−288.08	−293.67	−293.33	−293.48	−293.5[78]
CH_3CN	−286.39	−287.61	−293.03	−292.80	−292.96	−292.9[79]
CH_3**C**N	−286.25	−287.23	−293.01	−292.62	−292.77	−292.6[79]
O**C**S	−288.29	−289.43	−296.43	−295.44	−295.58	−295.2[80]
CO_2	−291.25	−292.24	−298.44	−297.45	−297.58	−297.7[81]
CO	−289.67	−290.76	−296.40	−295.91	−296.08	−296.2[82]
H_2**C**O	−288.14	−289.32	−295.01	−294.62	−294.79	−294.5[78]
Cl_2**C**O	−289.83	−290.93	−297.58	−296.66	−296.79	−296.8[78]
NH_3	−397.96	−399.20	−405.73	−405.77	−405.93	−405.6[83]
NF_3	−406.68	−407.86	−415.72	−414.64	−414.79	−414.2[83]
N$_2$	−402.11	−403.24	−410.07	−409.73	−409.88	−409.9[83]
N$_2$	−402.15	−403.29	−410.14	−409.72	−409.87	−409.9[83]
HC**N**	−398.34	−399.60	−407.02	−406.75	−406.91	−406.8[83]
ClC**N**	−397.39	−398.76	−406.75	−406.29	−406.45	−406.5[84]
CH_3C**N**	−396.83	−398.17	−405.96	−405.69	−405.86	−405.6[79]
OCS	−529.22	−530.80	−540.52	−540.22	−540.39	−540.3[80]
C**O**$_2$	−531.34	−532.71	−541.28	−541.03	−541.20	−541.3[81]
C**O**$_2$	−531.34	−532.71	−541.28	−541.19	−541.35	−541.3[81]
C**O**	−532.73	−534.00	−542.13	−542.25	−542.42	−542.6[82]
H_2C**O**	−529.18	−530.59	−539.22	−539.34	−539.55	−539.5[78]
Cl_2C**O**	−528.66	−530.22	−539.84	−539.56	−539.74	−539.7[78]
CEBEs						
MSE	7.9	6.7	−0.3	0.1	−0.1	
MAE	7.9	6.7	0.4	0.2	0.2	
CEBEs (with relativistic corrections) [b]						
MSE	7.8	6.6	−0.4	0.0	−0.2	
MAE	7.8	6.6	0.4	0.2	0.3	
Chemical shifts						
MSE	0.0	0.0	−0.1	0.1	0.1	
MAE	0.5	0.5	0.4	0.2	0.2	

[a] The reported CEBEs and chemical shifts correspond to the atoms in bold

[b] Relativisitic corrections of −0.06 eV, −0.13 eV, −0.25 and −0.45 eV were used for B, C, N, and O (1s)

of second-row elements.[31] However, with an MAE of 0.2 eV, *d*-GKS-spRPA performs even better without any semi-empirical adjustments to the energy functional. For *d*-GKS-spRPA, the change of potential from PBE to TPSS has no affect on the MAEs. For chemical shifts, *d*-GKS-spRPA maintains consistent accuracy with almost identical mean signed and mean absolute deviations for PBE and TPSS functionals, while *lin*-G_0W_0 has MAE of 0.5, 0.5 and 0.4 eV for PBE, TPSS, and BHLYP functionals, respectively. ΔSCF produces a MAE of 0.38 eV for CEBEs of organic molecules while ΔDFAs have MAE errors in the range of 0.16–0.24 eV depending on the choice of DFA.[85] The quality of chemical shifts from GKS-spRPA is thus similar to or better than Δ methods and *lin*-G_0W_0. Inclusion of relativistic corrections based on ΔSCF values,[72] changes the mean errors for CEBEs by ≤ 0.1 eV.

2. *Ammonia clusters*

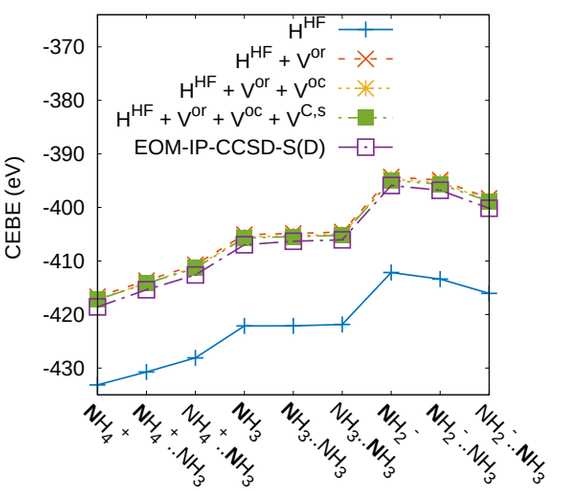

FIG. 1. N(1s) core-electron binding energies for ammonia clusters. The reported ionization potentials correspond to the atoms in bold. For *d*-GKS-spRPA calculations, we used PBE potential, def2-TZVPP basis sets, m5 grids, $\eta = 0.01$ a.u and $n_g = 400$. The molecular structures and EOM-IP-CCSD-S(D) values were taken from Ref. 73.

To further benchmark *d*-GKS-spRPA approach, we studied small ammonia clusters in different protonation states for which reference EOM-IP-CCSD-S(D) values[73] are available, see Fig. 1 and Table. II. Here the variations in CEBEs occur via changes in covalent and non-covalent effects. The former effect is due to changes in protonation states and

the latter due to clustering. The trends in reference CEBEs are adequately described by the H^{HF} component of the GKS-spRPA Hamiltonian, however the MAE for chemical shifts is 1.23 eV, see Table II. The inclusion of remaining three components of the GKS-spRPA Hamiltonian reduces the MAE in chemical shifts to 0.26 eV while maintaining the trends. Of the three components, V^{or} was the most important in reducing the MAE in chemical shifts. This study shows that *d*-GKS-spRPA adequately captures the chemical shifts due to variations in intramolecular- and intermolecular-bonding environments. Changing the KS potential from PBE to TPSS changes the chemical shifts by < 0.02 eV (see Table II and SI).

TABLE II. The N(1s) chemical shifts (in eV) of ammonia clusters using *d*-GKS-spRPA orbital energies. Contributions from H^{HF} (HF), $H^{HF} + V^{or}$ (+OR), and $H^{HF} + V^{or} + V^{oc}$ (+OC) to *d*-GKS-spRPA chemical shifts are also reported. MSE and MAE for the chemical shifts in each case are shown; the MSE is computed as the difference between theoretical and reference (Ref.) values obtained from EOM-IP-CCSD-S(D) method.[73] def2-TZVPP basis-sets, PBE potential, $n_g = 400$, $\eta = 0.01$ a.u. and m5 grids were used for d-GKS-spRPA calculations. The molecular geometries reported in Ref. 73 were used.

Molecule[a]	HF	+OR	+OC	*d*-GKS-spRPA	Ref.[73]
$\mathbf{N}H_4^+$	0.00	0.00	0.00	0.00	0.00
$\mathbf{N}H_4^+..NH_3$	2.42	3.01	3.02	3.02	3.20
$NH_4^+..\mathbf{N}H_3$	5.05	5.96	5.98	5.89	5.97
$\mathbf{N}H_3$	11.02	11.59	11.61	11.55	11.61
$\mathbf{N}H_3..NH_3$	11.03	11.82	11.84	11.77	12.27
$NH_3..\mathbf{N}H_3$	11.30	12.08	12.11	12.03	12.53
$\mathbf{N}H_2^-$	21.00	22.37	22.42	22.30	22.69
$\mathbf{N}H_2^-..NH_3$	19.76	21.78	21.84	21.59	21.78
$NH_2^-..\mathbf{N}H_3$	17.10	18.37	18.40	18.36	18.43
MSE	−1.23	−0.19	−0.16	−0.25	
MAE	1.23	0.19	0.17	0.25	

[a] The reported chemical shifts correspond to the atoms in bold

3. *Tautomers of Cytosine*

TABLE III. C(1s) CEBEs (in eV) of cytosine tautomers using *d*-GKS-spRPA, CVS-ADC(4) and experimental (Expt.) values. Only six resolved features are present in the experimental C(1s) spectrum.[86]

	d-GKS-spRPA[a]	CVS-ADC(4)[86]	Expt.[86]
B(C_5)	−290.45	−290.46	−290.6
A(C_5)	−290.77	−290.61	
C(C_5)	−291.00	−290.78	
B(C_6)	−291.81	−291.56	−291.7
A(C_6)	−292.58	−292.39	−292.4
C(C_6)	−292.69	−292.46	
B(C_4)	−293.23	−293.03	−293.2
A(C_4)	−293.41	−293.14	
C(C_4)	−293.31	−293.18	
B(C_2)	−293.89	−293.75	−293.9
A(C_2)	−294.08	−294.10	
C(C_2)	−295.16	−295.24	−295.1

[a] def2-TZVPP basis-sets, PBE potential, $n_g = 400$, $\eta = 0.01$ a.u. and m5 grids were used. The molecular geometries were optimized using PBE energy functional.

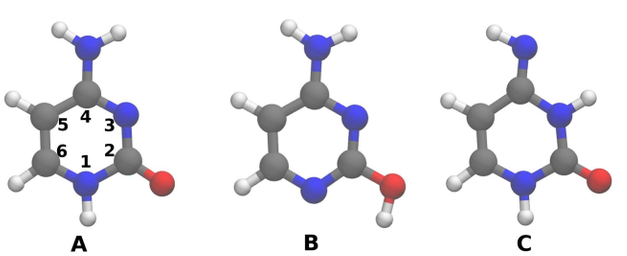

FIG. 2. Tautomers of cytosine considered in this study. The following color scheme was used for the atoms: H(white), C(grey), N (blue), and O(red).

Different protonation states can also result from tautomerization. Cytosine, for example, at $\sim$ 450K exists as three tautomers — A, B and C (Fig. 2) — as demonstrated in a

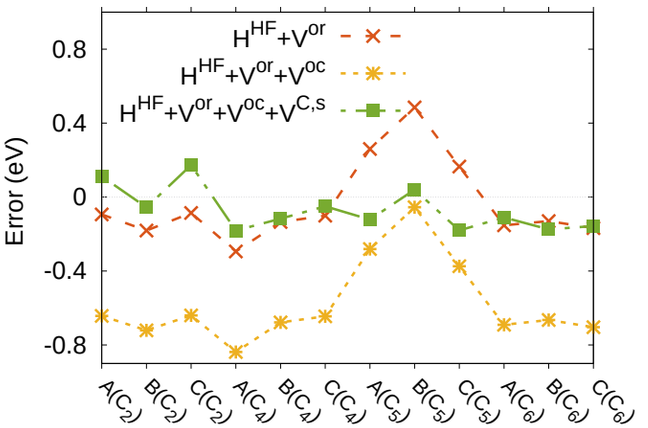

FIG. 3. Errors in *d*-GKS-spRPA based C(1s) CEBEs for cytosine tautomers. The reference values are from CVS-ADC(4).[86] For the *d*-GKS-spRPA calculations, def2-TZVPP basis-sets, PBE potential, $n_g = 400$, $\eta = 0.01$ a.u. and m5 grids were used. The molecular geometries were optimized using PBE energy functional.

combined experimental and theoretical study.[86] The study showed that the variations in the position of the proton in these three tautomers leads to only six resolved-features in the C(1s) XPS.(see Table III) Accurate simulation of the C(1s) XPS spectrum of cytosine is, therefore, a stringent test to the quality of any theoretical approach. The previous study showed that C(1s) theoretical spectrum obtained from shifted CVS-ADC(4) was in close agreement with the experiment indicating that the CVS-ADC(4) is a reliable benchmark for CEBEs of these tautomers.

For all three tautomers, we find that the *d*-GKS-spRPA based C(1s) CEBEs are within 0.2 eV of CVS-ADC(4) values. Unlike the case of ammonia clusters, here we find that $V^{C,s}$ component is crucial for reducing relative errors in CEBEs and MAE errors in chemical shifts, see Fig. 3. For example, inclusion of just $H^{HF} + V^{or}$ components leads to an error of 0.5 eV for B(C_5) (atom C_5 of tautomer B, see Fig. 2) while A(C_4) has an error of -0.3 eV, i.e. a relative error of 0.8 eV. The contribution of V^{oc} to the net CEBE is about 0.5 eV for each case and hence does not improve the relative errors. Similarly, any other constant shift to the CEBE will not lead to a reduction in the relative errors in CEBEs. The inclusion of $V^{C,s}$ component, however, reduces the maximum relative error to within 0.4 eV. We notice similar trends for MAE in chemical shifts, where we find that the $V^{C,s}$ component is crucial

for reducing the MAE to within 0.2 eV. Overall, this study underlines the importance of $V^{C,s}$ in describing subtle variations in CEBEs with changes in covalent-bonding environment.

B. Solvation induced chemical shifts

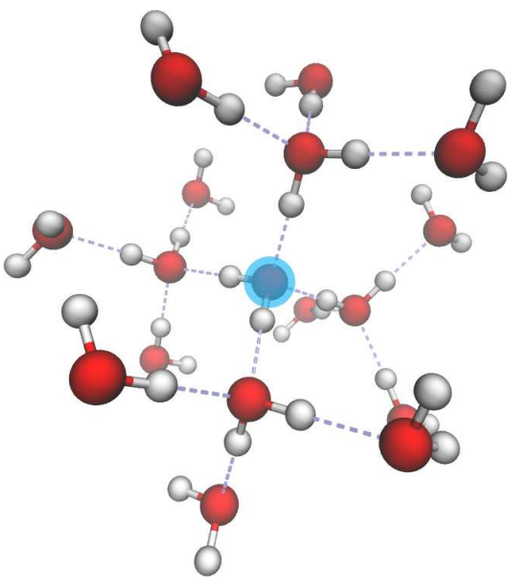

FIG. 4. $(H_2O)_{17}$ cluster from ice-Ih structure.[87] The reported chemical shifts correspond to the O(1s) of central water molecule (highlighted in blue).

Finally, we use the *d*-GKS-spRPA approach to analyze the impact of solvation on chemical shifts. As a pilot application we studied the change in O(1s) CEBE of water molecules from the gas (H_2O(g)) to liquid (H_2O(l)) and solid (H_2O(s)) phases. This study is important given the increasing number of liquid-jet XPS experiments being carried out in aqueous medium. Unlike for the previous cases, the chemical shifts due to hydration result solely from non-covalent hydrogen-bonding interactions and dielectric screening. While the impact of hydrogen-bonding is captured by the electrostatic contribution from H^{HF}, the impact of dielectric screening is captured by the remaining terms of H^{RPA}. To model the CEBE of H_2O(s) we use a single cluster cut-out from the Ih phase of ice (Fig. 4), and for modeling H_2O(l) we use 22 clusters cut-out from a molecular dynamics (MD) snapshot.[88] For each of these clusters, we focus on a central water molecule as a representative of the bulk solvated state.

TABLE IV. Individual and total contributions to the *d*-GKS-spRPA chemical shifts (eV) of Ice-Ih clusters, $(H_2O)_n$. The calculations were carried out using PBE potential, def2-TZVPP basis sets, m5 grids, $n_g = 60$ and $\eta = 0.01$ a.u. The reported shifts correspond to the difference of the O(1s) CEBEs of the central-water molecule in the cluster and in its isolated gas-phase form.

$n =$	H^{HF}	V^{or}	V^{oc}	$V^{C,s}$	Total
5	0.28	1.13	0.00	−0.02	1.39
17	0.18	1.47	0.00	−0.02	1.62

1. Ice-Ih

For ice-Ih, we are unaware of any available estimates of O(1s) chemical shifts w.r.t gas phase water. But given the well-defined O-atom lattice for ice, compared to H_2O(l), we can analyze the impact of various solvation shells on the chemical shift. This will be insightful for studying H_2O(l) discussed below. To model the chemical shift, we use a $(H_2O)_{17}$ cluster, consisting of a central water molecule, surrounded by four water molecules which are hydrogen-bonded to it. Each of these four water molecules are hydrogen-bonded to three other water molecules, see Fig. 4. For this model, the *d*-GKS-spRPA O(1s) chemical shift w.r.t the isolated central water molecule is 1.62 eV, see Table. IV. Including only the first hydrogen-bonding shell leads to a shift of 1.39 eV of which H^{HF} contributes about 0.28 eV, V^{R} contributes about -0.02 eV, while V^{or} contributes about 1.13 eV. The orbital-correlation component, V^{oc}, remains the same upon the inclusion of additional water molecules, and hence does not contribute to the chemical shift. The addition of the second hydrogen-bonding shell increases the chemical shift by 0.23 eV ; of this change H^{HF} contributes -0.10 eV and V^{R} contributes 0.34 eV. We estimate that the addition of next-set of hydrogen-bonding water molecules does not change the chemical shift. We thus see that (i) the major fraction of the chemical shift results from the dielectric effects of water-medium (estimated using the V^{or} term), and the effect of hydrogen-bonding is secondary (estimated using H^{HF} term); inclusion of these two components, i.e. the orbital-relaxation-only approximation, is sufficient for studies of chemical shift of water clusters, and (ii) inclusion of the first and second hydrogen-bonding shells (which approximately equals the size of second hydration-shell) is sufficient to account for the chemical shift. Using a non-polarizable SPC

point-charge model[89] to represent the second hydrogen-bonding shell led to no significant change in the binding energies, suggesting that at least polarizable-models may be necessary to represent the chemical environmental effects.

TABLE V. Chemical shifts (eV), computed using the orbital-relaxation-only approximation ($H^{HF} + V^{or}$), of 22 water clusters, for different radial sizes (R (in Å)) of the clusters. For $R = 5.0$ Å we use def2-TZVPP basis sets, while for larger clusters we use a combination of def2-SVP and def2-TZVPP basis sets to obtain the chemical shifts. All calculations were carried out using PBE potential and m5 grids. Reported shifts correspond to the difference between the O(1s) CEBEs for central water molecule in the cluster and gas-phase.

Shift	R (in Å)		
	5.0	5.5	6.0
Avg.	1.52	1.64	1.65
Max.	2.63	2.75	2.59
Min.	0.26	0.15	0.26

2. *Liquid water*

For H_2O(l), the liquid-jet XPS experiments by us (in the present work, see SI for experimental details) and that by Winter et al.[90] indicate an O(1s) chemical shift of 2.0 eV and 1.8 eV, respectively, w.r.t H_2O(g). An XPS study of large water clusters indicates that the chemical shift is 1.6 eV.[91] To model this shift we use 22 water clusters that were cut-out of a snapshot obtained from a classical MD simulation using the SPC-water model.[89] Each cluster was constructed by randomly selecting a central water molecule from the MD snapshot, and then selecting all water molecules present within a certain radius, R, of the selected central water molecule. For a chosen R we computed the chemical shift of the central water-molecule in the cluster w.r.t its isolated form (i.e. no geometry relaxation between the cluster and isolated forms). Only $H^{HF} + V^{or}$ components were included in the estimation of chemical shifts as other components were unimportant for water clusters(Sec. IV B 1). The average chemical shift for these 22 clusters w.r.t R converges to 1.65 eV, see Table V, which is within reported range of experimental values (1.6–2.0 eV), and indicates the suitability

of our methods for studies of chemical shifts in liquids. A more reliable estimate would require better sampling and use of MD simulations based on accurate force-fields or ab initio methods.[92]

V. CONCLUSIONS

GKS-spRPA orbital energies yield CEBEs that are more accurate than those from linearized *GW* theory at comparable computational cost without any empirical adjustments. From a many-body perturbation theory viewpoint, the success of GKS-spRPA for CEBEs can be rationalized by correlation and relaxation contributions beyond second-order captured by GKS-spRPA orbital energies. Furthermore, the accuracy of GKS-spRPA does not rely on the scale-dependent error cancellation between approximate exchange and correlation typical of semi-local DFAs, thus producing uniformly accurate results for valence and core states with vastly different density scales and interaction strengths. Compared to traditional Δ methods, GKS-spRPA has the distinct advantage of variational stability. For the systems investigated here, GKS-spRPA CEBEs agree with EOM-CCSD-IP and ADC(4) results within a few tenths of an eV. GKS-spRPA orbital energies are less sensitive to the choice of DFA for the KS potential than conventional KS or GKS results, but further steps towards complete independence from a DFA reference are desirable.[50]

Our results for water in different environments suggest that GKS-spRPA is a useful tool for interpreting the results of XPS experiments in complex systems such as liquids or interfaces. The relatively moderate computational cost of GKS-spRPA allows for calculations including explicit solvent in conjunction with MD simulations. The relative importance of dielectric screening, hydrogen bonding, or electrostatic interaction can be assessed using the partitioning scheme introduced in this work. The results for cytosine and ammonia clusters illustrate that GKS-spRPA chemical shifts capture subtle variations in covalent and noncovalent bonding environment within solvents, for e.g., due to changes in pH or intermolecular association.

SUPPLEMENTARY MATERIAL

See supplementary material for parameter and basis-sets dependency tests of GKS-spRA; CEBEs of small molecules, ammonia clusters, cytosine tautomers and water clusters; cartesian coordinates of small molecule testset, cytosine tautomers, and ice cluster.

ACKNOWLEDGMENTS

We thank Sree Ganesh Balasubramani and Prof. Ravindra Venkatramani for helpful suggestions. This material is based upon work supported by the National Science Foundation under CHE-1800431. The lab based liquid-jet ambient pressure photoelectron spectrometer used to acquire the XPS spectra of liquid water shown in the SI was obtained through a grant from the W. M. Keck Foundation.

The authors declare the following competing financial interest(s): Principal Investigator Filipp Furche has an equity interest in Turbomole GmbH. The terms of this arrangement have been reviewed and approved by the University of California, Irvine, in accordance with its conflict of interest policies.

REFERENCES

[1]K. Siegbahn, Nobel Lecture: Electron Spectroscopy for Atoms, Molecules and Condensed Matter (1981).

[2]M. Faubel, S. Schlemmer, and J. P. Toennies, Z. Phys. D **10**, 269 (1988).

[3]M. Faubel and B. Steiner, Phys. Chem. **96**, 1167 (1992).

[4]T. Buttersack, P. E. Mason, R. S. McMullen, T. Martinek, K. Brezina, D. Hein, H. Ali, C. Kolbeck, C. Schewe, S. Malerz, B. Winter, R. Seidel, O. Marsalek, P. Jungwirth, and S. E. Bradforth, J. Am. Chem. Soc. **141**, 1838 (2019), pMID: 30673221.

[5]S. Ghosal, J. C. Hemminger, H. Bluhm, B. S. Mun, E. L. D. Hebenstreit, G. Ketteler, D. F. Ogletree, F. G. Requejo, and M. Salmeron, Science **307**, 563 (2005).

[6]B. Winter, Nucl. Instrum. Meth. A **601**, 139 (2009).

[7]B. Winter and M. Faubel, Chem. Rev. **106**, 1176 (2006).

[8]M. A. Brown, M. Faubel, and B. Winter, Annu. Rep. Prog. Chem., Sect. C: Phys. Chem. **105**, 174 (2009

[9]F. Viñes, C. Sousa, and F. Illas, Phys. Chem. Chem. Phys. **20**, 8403 (2018).

[10]A. Proctor and P. M. A. Sherwood, Anal. Chem. **54**, 13 (1982).

[11]C. Chang, M. Pelissier, and P. Durand, Phys. Scr. **34**, 394 (1986).

[12]E. v. Lenthe, E. J. Baerends, and J. G. Snijders, J. Chem. Phys. **99**, 4597 (1993).

[13]L. Hedin and A. Johansson, J. Phys. B: At. Mol. Phys **2**, 1336 (1969).

[14]P. S. Bagus, E. S. Ilton, and C. J. Nelin, Surf. Sci. Rep. **68**, 273 (2013).

[15]P. S. Bagus and H. F. Schaefer III, J. Chem. Phys. **55**, 1474 (1971).

[16]P. S. Bagus, Phys. Rev. **139**, A619 (1965).

[17]J. Shim, M. Klobukowski, M. Barysz, and J. Leszczynski, Phys. Chem. Chem. Phys. **13**, 5703 (2011).

[18]A. Görling, Phys. Rev. A **59**, 3359 (1999).

[19]C. Kolczewski, R. Püttner, O. Plashkevych, H. Ågren, V. Staemmler, M. Martins, G. Snell, A. S. Schlachter, M. Sant'Anna, G. Kaindl, and L. G. M. Pettersson, J. Chem. Phys. **115**, 6426 (2001).

[20]D. A. Shirley, Chem. Phys. Lett. **16**, 220 (1972).

[21]J. Schirmer, L. S. Cederbaum, and O. Walter, Phys. Rev. A **28**, 1237 (1983).

[22]M. Nooijen and R. J. Bartlett, J. Chem. Phys. **102**, 3629 (1995).

[23]J. F. Stanton and J. Gauss, J. Chem. Phys. **101**, 8938 (1994).

[24]G. Angonoa, O. Walter, and J. Schirmer, J. Chem. Phys. **87**, 6789 (1987).

[25]J. Schirmer and A. Thiel, J. Chem. Phys. **115**, 10621 (2001).

[26]A. Thiel, J. Schirmer, and H. Köppel, J. Chem. Phys. **119**, 2088 (2003).

[27]L. S. Cederbaum, W. Domcke, and J. Schirmer, Phys. Rev. A **22**, 206 (1980).

[28]L. Hedin, Phys. Rev. **139**, A796 (1965).

[29]F. Aryasetiawan and O. Gunnarsson, Rep. Prog. Phys. **61**, 237 (1998).

[30]M. J. van Setten, R. Costa, F. Viñes, and F. Illas, J. Chem. Theory Comput. **14**, 877 (2018).

[31]D. Golze, J. Wilhelm, M. J. van Setten, and P. Rinke, J. Chem. Theory Comput. **14**, 4856 (2018).

[32]W. Kohn and L. J. Sham, Phys. Rev. **140**, A1133 (1965).

[33]M. Dauth, F. Caruso, S. Kümmel, and P. Rinke, Phys. Rev. B **93**, 121115 (2016).

[34]F. Caruso, M. Dauth, M. J. van Setten, and P. Rinke, J. Chem. Theory Comput. **12**, 5076 (2016).

[35]S. V. Faleev, M. van Schilfgaarde, and T. Kotani, Phys. Rev. Lett. **93**, 126406 (2004).

[36]A. Stan, P. Romaniello, S. Rigamonti, L. Reining, and J. A. Berger, New J. Phys. **17**, 093045 (2015).

[37]M. Véril, P. Romaniello, J. A. Berger, and P.-F. Loos, J. Chem. Theory Comput. **14**, 5220 (2018).

[38]F. Tandetzky, J. K. Dewhurst, S. Sharma, and E. K. U. Gross, Phys. Rev. B **92**, 115125 (2015).

[39]A. Seidl, A. Görling, P. Vogl, J. A. Majewski, and M. Levy, Phys. Rev. B **53**, 3764 (1996).

[40]J. F. Janak, Phys. Rev. B **18**, 7165 (1978).

[41]W. Yang, A. J. Cohen, and P. Mori-Sánchez, J. Chem. Phys. **136**, 204111 (2012).

[42]T. Koopmans, Physica **1**, 104 (1934).

[43]J. P. Perdew, R. G. Parr, M. Levy, and J. L. Balduz, Phys. Rev. Lett. **49**, 1691 (1982).

[44]C.-O. Almbladh and U. von Barth, Phys. Rev. B **31**, 3231 (1985).

[45]A. J. Cohen, P. Mori-Sánchez, and W. Yang, Phys. Rev. B **77**, 115123 (2008).

[46]J. P. Perdew, K. Burke, and M. Ernzerhof, Phys. Rev. Lett. **77**, 3865 (1996).

[47]C. Lee, W. Yang, and R. G. Parr, Phys. Rev. B **37**, 785 (1988).

[48]A. D. Becke, J. Chem. Phys. **98**, 5648 (1993).

[49]N. Pueyo Bellafont, P. S. Bagus, and F. Illas, J. Chem. Phys. **142**, 214102 (2015).

[50]V. K. Voora, S. G. Balasubramani, and F. Furche, Phys. Rev. A **99**, 012518 (2019).

[51]D. C. Langreth and J. P. Perdew, Solid State Commun. **17**, 1425 (1975).

[52]D. Langreth and J. Perdew, Phys. Rev. B **15**, 2884 (1977).

[53]O. Gunnarsson and B. I. Lundqvist, Phys. Rev. B **13**, 4274 (1976).

[54]H. Eshuis, J. Yarkony, and F. Furche, J. Chem. Phys. **132**, 234114 (2010).

[55]H. Eshuis, J. E. Bates, and F. Furche, Theor. Chem. Acc. **131**, 1084 (2012).

[56]J. Toulouse, I. C. Gerber, G. Jansen, A. Savin, and J. G. Ángyán, Phys. Rev. Lett. **102**, 096404 (2009).

[57]A. L. Fetter and J. D. Walecka, *Quantum theory of many-particle systems* (Dover Publications Inc., New York, 2003).

[58]J. P. Boyd, J. Sci. Comput. **2**, 99 (1987).

[59]G. Born, H. A. Kurtz, and Y. Öhrn, J. Chem. Phys. **68**, 74 (1978).

[60]B. Pickup and O. Goscinski, Mol. Phys. **26**, 1013 (1973).

[61]A. Szabo and N. S. Ostlund, *Modern quantum chemistry: introduction to advanced electronic structure theory* (Courier Corporation, 2012).

[62]A. M. Burow, J. E. Bates, F. Furche, and H. Eshuis, J. Chem. Theory Comput. **10**, 180 (2014).

[63]M. Deleuze, M. K. Scheller, and L. S. Cederbaum, J. Chem. Phys. **103**, 3578 (1995).

[64]L. S. Cederbaum and W. Domcke, "Theoretical aspects of ionization potentials and photoelectron spectroscopy: A green's function approach," in *Adv. Chem. Phys.* (John Wiley & Sons, Ltd, 2007) pp. 205–344.

[65]Y. Öhrn and J. Ortiz, Mol. Phys. **108**, 2871 (2010).

[66]F. Furche, R. Ahlrichs, C. Hättig, W. Klopper, M. Sierka, and F. Weigend, WIREs Comput. Mol. Sci. **4**, 91 (2014).

[67]A. D. Becke, J. Chem. Phys. **98**, 1372 (1993).

[68]J. Tao, J. P. Perdew, V. N. Staroverov, and G. E. Scuseria, Phys. Rev. Lett. **91**, 146401 (2003).

[69]"Turbomole v7.3 2018, a development of university of karlsruhe and forschungszentrum karlsruhe gmbh

[70]M. J. van Setten, F. Weigend, and F. Evers, J. Chem. Theory Comput. **9**, 232 (2013).

[71]O. Treutler and R. Ahlrichs, J. Chem. Phys. **102**, 346 (1995).

[72]N. Pueyo Bellafont, F. Viñes, and F. Illas, J. Chem. Theory Comput. **12**, 324 (2016).

[73]A. Sadybekov and A. I. Krylov, J. Chem. Phys. **147**, 014107 (2017).

[74]F. Weigend and R. Ahlrichs, Phys. Chem. Chem. Phys. **7**, 3297 (2005).

[75]T. H. Dunning, J. Chem. Phys. **90**, 1007 (1989).

[76]K. A. Peterson and C. Puzzarini, Theor. Chem. Acc. **114**, 283 (2005).

[77]D. A. Allison, G. Johansson, C. J. Allan, U. Gelius, H. Siegbahn, J. Allison, and K. Siegbahn, J. Electon. Spectrosc. Relat. Phenom. **1**, 269 (1972).

[78]W. L. Jolly, K. D. Bomben, and C. J. Eyermann, At. Data and Nucl. Data Tables **31**, 433 (1984).

[79]A. Naves de Brito, S. Svensson, H. Ågren, and J. Delhalle, J. Electon. Spectrosc. Relat. Phenom. **63**, 239 (1993).

[80]C. J. Allan, U. Gelius, D. A. Allison, G. Johansson, H. Siegbahn, and K. Siegbahn, J. Electon. Spectrosc. Relat. Phenom. **1**, 131 (1972).

[81]T. D. Thomas and R. W. Shaw Jr., J. Electon. Spectrosc. Relat. Phenom. **5**, 1081 (1974).

[82]S. R. Smith and T. Darrah Thomas, J. Electon. Spectrosc. Relat. Phenom. **8**, 45 (1976).

[83]W. L. Jolly, P. Finn, R. K. Pearson, and J. M. Hollander, Inorg. Chem. **10**, 378 (1971).

[84]J. M. Buschek, F. S. Joergensen, and R. S. Brown, J. Am. Chem. Soc. **104**, 5019 (1982).

[85]N. Pueyo Bellafont, G. Álvarez Saiz, F. Viñes, and F. Illas, Theor. Chem. Acc. **135**, 35 (2016).

[86]V. Feyer, O. Plekan, R. Richter, M. Coreno, G. Vall-llosera, K. C. Prince, A. B. Trofimov, I. L. Zaytseva, T. E. Moskovskaya, E. V. Gromov, and J. Schirmer, J. Phys. Chem. A **113**, 5736 (2009).

[87]W. F. Kuhs and M. S. Lehmann, J. Phys. Chem. **87**, 4312 (1983).

[88]Taken from http://ergoscf.org/xyz/h2o.php.

[89]H. J. Berendsen, J. P. Postma, W. F. van Gunsteren, and J. Hermans, in *Intermolecular forces* (Springer, 1981) pp. 331–342.

[90]B. Winter, E. F. Aziz, U. Hergenhahn, M. Faubel, and I. V. Hertel, J. Chem. Phys. **126**, 124504 (2007).

[91]G. Öhrwall, R. F. Fink, M. Tchaplyguine, L. Ojamäe, M. Lundwall, R. R. T. Marinho, A. Naves de Brito, S. L. Sorensen, M. Gisselbrecht, R. Feifel, T. Rander, A. Lindblad, J. Schulz, L. J. Sæthre, N. Mårtensson, S. Svensson, and O. Björneholm, J. Chem. Phys. **123**, 054310 (2005).

[92]T. A. Pham, X. Zhang, B. C. Wood, D. Prendergast, S. Ptasinska, and T. Ogitsu, J. Phys. Chem. Lett. **9**, 194 (2018).

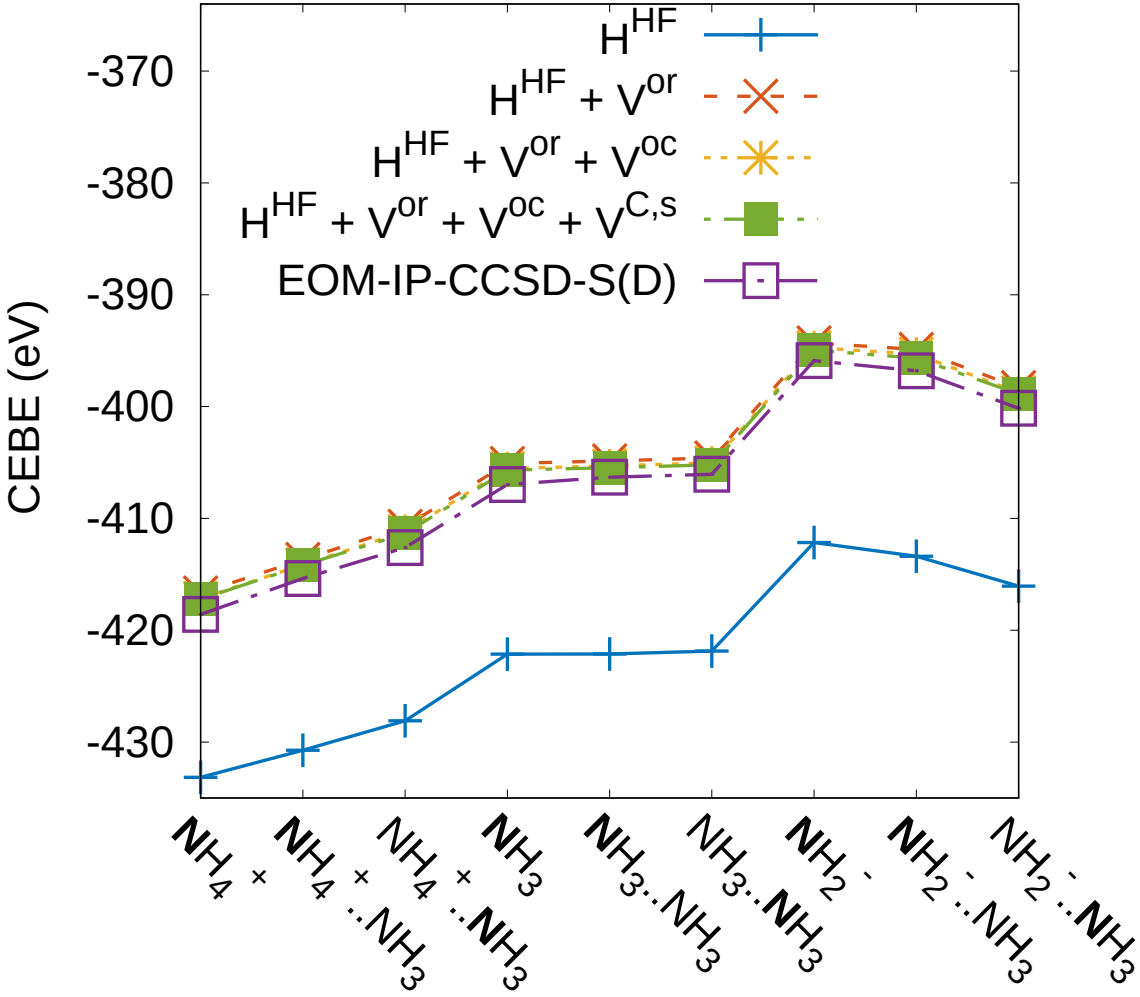
CEBE (eV)
-370
-380
-390
-400
-410
-420
-430
H^HF
H^HF + V^or
H^HF + V^or + V^oc
H^HF + V^or + V^oc + V^C,s
EOM-IP-CCSD-S(D)
NH4 +
NH4 + ..NH3
NH4 + ..NH3
NH3
NH3..NH3
NH3..NH3
NH2 -
NH2 - ..NH3
NH2 - ..NH3

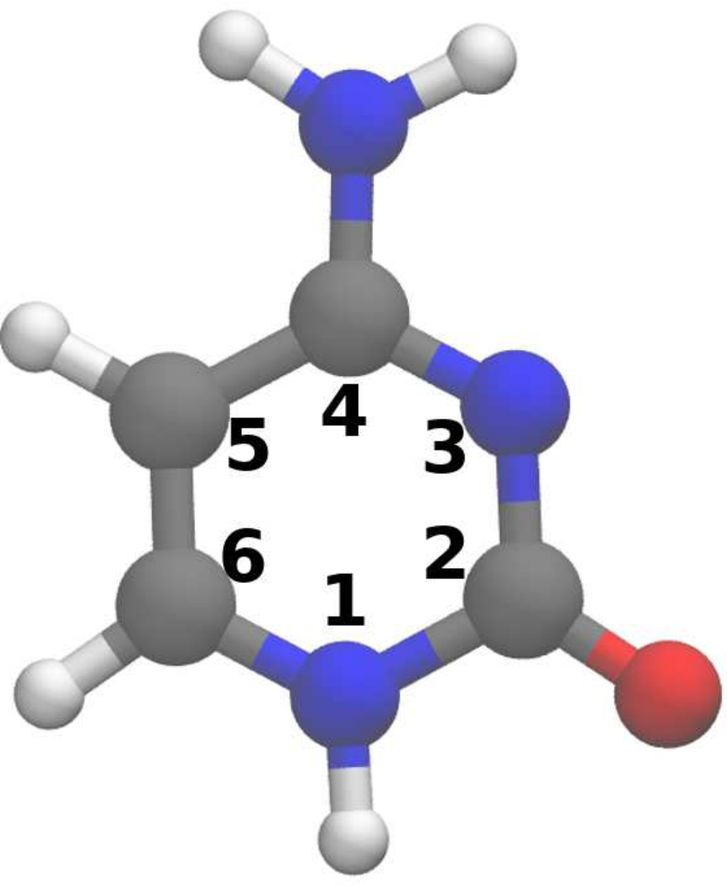

A

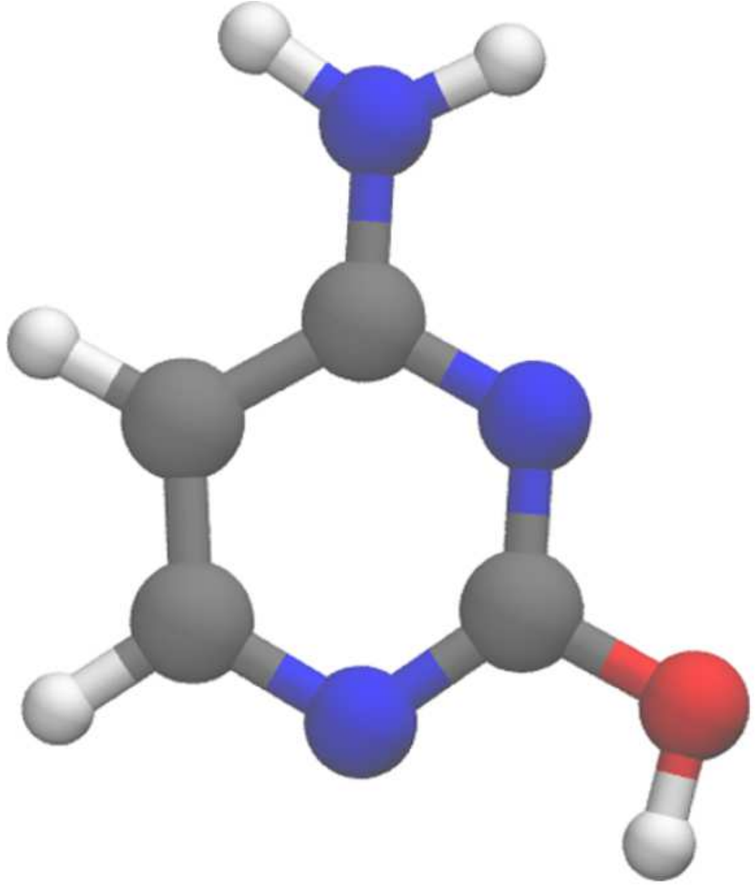

B

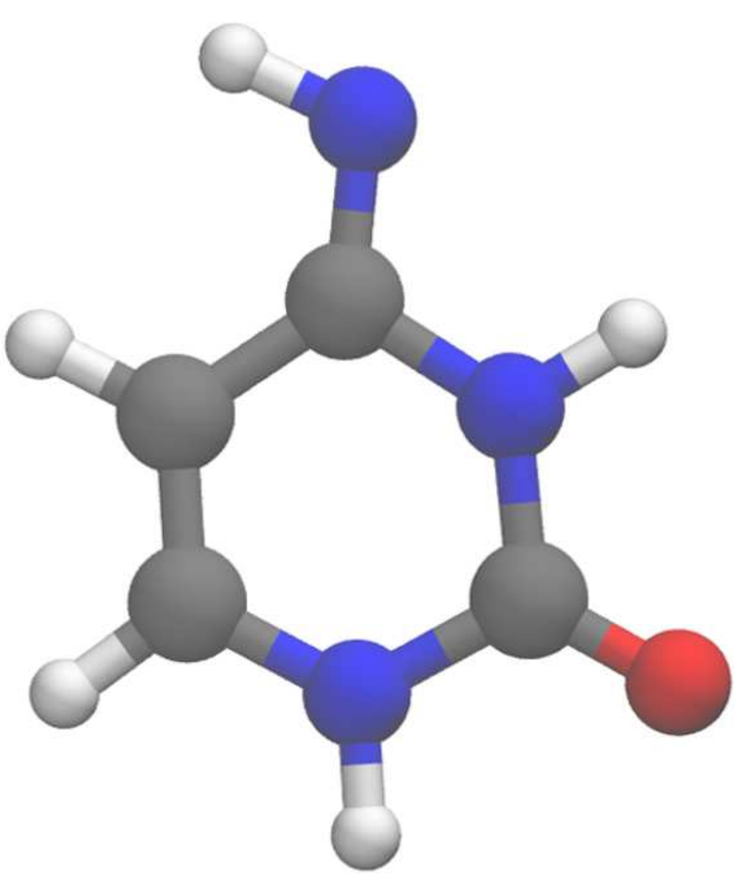

C

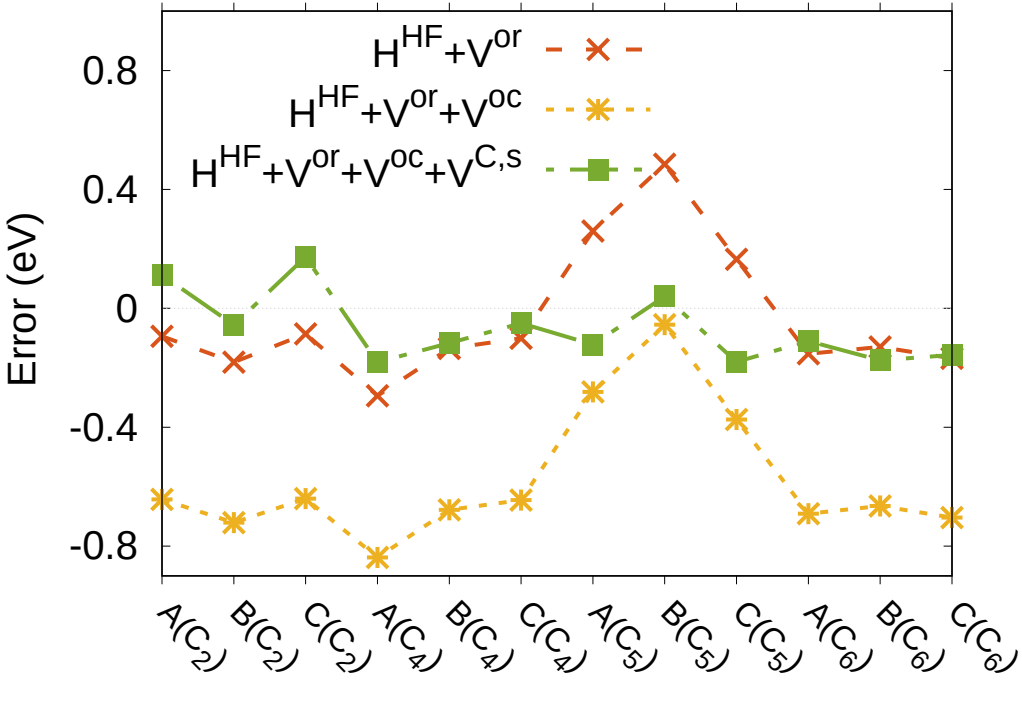
H^HF+V^or
H^HF+V^or+V^oc
H^HF+V^or+V^oc+V^C,s
Error (eV)
0.8
0.4
0
-0.4
-0.8
A(C2)
B(C2)
C(C2)
A(C4)
B(C4)
C(C4)
A(C5)
B(C5)
C(C5)
A(C6)
B(C6)
C(C6)